Journal of Experimental Botany
https://doi.org/10.1093/jxb/erad454 Advance Access Publication 17 November 2023

RESEARCH PAPER

Arabidopsis PHYTOALEXIN DEFICIENT 4 promotes the maturation and nuclear accumulation of immune-related cysteine protease RD19

Yanhong Zeng[1,†], Zichao Zheng[1,†], Giuliana Hessler[2], Ke Zou[1], Junchen Leng[1], Jaqueline Bautor[2], Johannes Stuttmann[3], Li Xue[4], Jane E. Parker[2,5], and Haitao Cui[1,6,*]

[1] State Key Laboratory Key Laboratory of Ecological Control of Fujian-Taiwan Crop Pests, Plant Immunity Center, Fujian Agriculture and Forestry University, Fuzhou 350002, China
[2] Department of Plant-Microbe Interactions, Max-Planck Institute for Plant Breeding Research, Carl-von-Linne Weg 10, 50829 Cologne, Germany
[3] CEA, CNRS, BIAM, UMR7265, LEMiRE (Rhizosphère et Interactions sol-plante-microbiote), Aix Marseille University, 13115 Saint-Paul lez Durance, France
[4] College of Chemistry and Life Sciences, Zhejiang Normal University, Jinhua 321004, China
[5] Cologne-Duesseldorf Cluster of Excellence on Plant Sciences (CEPLAS), 40225 Duesseldorf, Germany
[6] Shandong Provincial Key Laboratory of Agricultural Microbiology, College of Plant Protection, Shandong Agricultural University, Tai'an, Shandong 271018, China

[†] These authors contributed equally to this work.
[*] Correspondence: cuihaitao@sdau.edu.cn

Received 24 May 2023; Editorial decision 6 November 2023; Accepted 16 November 2023

Editor: Daolong Dou, Nanjing Agricultural University, China

Abstract

Arabidopsis PHYTOALEXIN DEFICIENT 4 (PAD4) has an essential role in pathogen resistance as a heterodimer with ENHANCED DISEASE SUSCEPTIBILITY 1 (EDS1). Here we investigated an additional PAD4 role in which it associates with and promotes the maturation of the immune-related cysteine protease RESPONSIVE TO DEHYDRATION 19 (RD19). We found that RD19 and its paralog RD19c promoted EDS1- and PAD4-mediated effector-triggered immunity to an avirulent *Pseudomonas syringae* strain, DC3000, expressing the effector AvrRps4 and basal immunity against the fungal pathogen *Golovinomyces cichoracearum*. Overexpression of RD19, but not RD19 protease-inactive catalytic mutants, in Arabidopsis transgenic lines caused EDS1- and PAD4-dependent autoimmunity and enhanced pathogen resistance. In these lines, RD19 maturation to a pro-form required its catalytic residues, suggesting that RD19 undergoes auto-processing. In transient assays, PAD4 interacted preferentially with the RD19 pro-protease and promoted its nuclear accumulation in leaf cells. Our results lead us to propose a model for PAD4-stimulated defense potentiation. PAD4 promotes maturation and nuclear accumulation of processed RD19, and RD19 then stimulates EDS1–PAD4 dimer activity to confer pathogen resistance. This study highlights potentially important additional PAD4 functions that eventually converge on canonical EDS1–PAD4 dimer signaling in plant immunity.

Keywords: Cysteine protease, EDS1, effector triggered immunity, nucleus, PAD4, resistance.

Introduction

In terrestrial environments plants encounter pathogens with elaborate strategies to exploit the plant as a host. In turn, plants have evolved receptors to detect pathogen attack and activate defense pathways that limit infection. Large families of plasma membrane localized receptor-like kinase (RLK) and receptor-like protein (RLP) proteins intercept pathogen- or damage-derived molecules to confer pattern-triggered immunity (PTI) (Albert *et al.*, 2020). Microbial strains that have become adapted to a particular host deliver virulence factors (effectors) to host cells that promote their colonization, often by disabling PTI. A further recognition layer is provided by intracellular nucleotide-binding/leucine-rich repeat (NLR) immune receptors that detect specific effector molecules or effector-mediated modifications of host components to confer a stronger defense response called effector-triggered immunity (ETI) (Cui *et al.*, 2015; Jones *et al.*, 2016). ETI often culminates in localized host programmed cell death (the hypersensitive response).

In PTI, activated RLK or RLP receptors function with co-receptors to initiate intracellular phosphorylation and Ca^{2+}-dependent signaling cascades promoting apoplastic and transcriptional defenses (Albert *et al.*, 2020; Koster *et al.*, 2022). In ETI, two major classes of effector-sensing NLR receptors—coiled-coil (CC) domain NLRs (CNLs) and Toll–Interleukin-1 Receptor (TIR) domain NLRs (TNLs)—form effector-induced oligomers called resistosomes (Hu and Chai, 2023). In the respective resistosome complexes, N-terminal CC and TIR domains re-arrange for signaling (Hu and Chai, 2023). The CNL resistosomes Arabidopsis HOPZ-ACTIVATED RESISTANCE1 (ZAR1) and wheat STEM RUST35 (Sr35) are pentamers with CC domain-encoded Ca^{2+}-permeable ion channel activity at the plasma membrane (Wang *et al.*, 2019; Bi *et al.*, 2021; Forderer *et al.*, 2022). CNL channel-induced Ca^{2+} ion fluxes presumably stimulate intracellular Ca^{2+}-dependent protein kinases and transcription factors to confer ETI (Kim *et al.*, 2022; Parker *et al.*, 2022; Jiang and Ding, 2023). By contrast, the TNL resistosomes Arabidopsis RECOGNITION of PERONOSPORA PARASITICA1 (RPP1) and *Nicotiana benthamiana* RECOGNITION of XOPQ1 (Roq1) are tetramers with TIR domain-encoded NADase activity (Ma *et al.*, 2020; Martin *et al.*, 2020). ETI and PTI receptor systems can cross-potentiate each other to amplify defense signaling cascades and ETI-associated host cell death (Ngou *et al.*, 2021; Tian *et al.*, 2021; Yuan *et al.*, 2021).

Emerging evidence shows that CNL resistosomes trigger ETI-associated cell death and pathogen resistance autonomously (Wang *et al.*, 2019; Bi *et al.*, 2021; Forderer *et al.*, 2022) or through their activation of related CNL-type 'helper' NLRs (Ahn *et al.*, 2023; Contreras *et al.*, 2023). By contrast, TNL receptors recruit a small conserved family of lipase-like proteins, ENHANCED DISEASE SUSCEPTIBILITY1 (EDS1), PHYTOALEXIN DEFICIENT4 (PAD4) and SENESCENCE ASSOCIATED GENE101 (SAG101), to promote ETI by activating two sub-classes of conserved CNL-like (CC^R) helper NLRs, ACTIVATED DISEASE RESISTANCE1 (ADR1) and N REQUIREMENT GENE1 (NRG1) (Lapin *et al.*, 2020; Sun *et al.*, 2021; Wu *et al.*, 2021). NADase-active TNLs as well as TIR-domain proteins [TIRs; such as Arabidopsis RESPONSE to HOPBA1 (RBA1)] produce particular NAD^+ catalytic products (ribosylated nucleotides) that preferentially bind to EDS1–PAD4 or EDS1–SAG101 heterodimers, enabling their specific association with co-functioning ADR1 or NRG1 helper NLRs to confer immunity (Dongus *et al.*, 2022; Huang *et al.*, 2022; Jia *et al.*, 2022, 2023; Locci *et al.*, 2023). Whereas the EDS1–SAG101–NRG1 node appears to be dedicated to TNL-mediated ETI in dicot plants (Gantner *et al.*, 2019; Lapin *et al.*, 2019, 2022; Sun *et al.*, 2021), studies show that the EDS1–PAD4–ADR1 node is more broadly recruited for transcriptional defense potentiation, stimulated by TNL, CNL and certain PRR receptors (Dongus and Parker, 2021; Lapin *et al.*, 2022). EDS1 provides an essential scaffold for TIR/TNL-induced PAD4 association with ADR1 helper NLRs (Wagner *et al.*, 2013; Huang *et al.*, 2022). Notably, Arabidopsis PAD4 has an EDS1-independent role in promoting defenses that limit aphid feeding (Pegadaraju *et al.*, 2007; Louis *et al.*, 2012; Dongus *et al.*, 2020). We therefore postulated that Arabidopsis PAD4 has additional resistance-promoting activities that remain to be uncovered.

In this study, we characterized an interaction between Arabidopsis PAD4 and the papain-like cysteine protease (PLCP) RESPONSIVE TO DEHYDRATION 19 (RD19), which was identified through immunoprecipitation of PAD4 followed by protein identification with mass spectrometry. In plants, PLCPs contribute to both cell-surface receptor- and NLR-mediated immunity (van der Hoorn, 2008; Liu *et al.*, 2018). Most studied PLCPs are secreted to the apoplast where they promote immune responses either as pathogen virulence targets or decoys that are guarded by cell-surface receptors (Paulus *et al.*, 2020; Godson and van der Hoorn, 2021). PLCPs can also generate immunogenic peptides that could be recognized by cell-surface receptors (Ziemann *et al.*, 2018). The discovery of PLCPs as pathogen effector targets to promote infection underscores their importance in immunity regulation (Rooney *et al.*, 2005; Ilyas *et al.*, 2015; Pogorelko *et al.*, 2019). Arabidopsis RD19 was found to promote bacterial effector PSEUDOMONAS OUTER PROTEIN P2 (PopP2)-triggered TNL (RESISTANT TO RALSTONIA SOLANACEARUM 1/RESISTANT TO P. SYRINGAE 4, RRS1/RPS4) ETI to *Ralstonia solanacearum* root-infecting bacteria (Bernoux *et al.*, 2008). PopP2 is an acetyltransferase that, through its enzymatic activity, disables defensive WRKY transcription factor binding to the chromatin, which is recognized by an Arabidopsis nuclear TNL pair, RRS1/RPS4, to activate ETI (Le Roux *et al.*, 2015; Sarris *et al.*, 2015). In transient *N. benthamiana* expression assays, PopP2 associated with RD19

and promoted RD19 re-localization from vacuoles to the nucleus (Bernoux *et al.*, 2008). Here we show that a structure-guided N-terminal domain variant of PAD4 ($PAD4^{MLF}$) (Wagner *et al.*, 2013) that retains extremely weak interaction with EDS1 *in vivo* is, unexpectedly, fully functional in TNL immunity. Using immunoprecipitation followed by protein identification with mass spectrometry of non-triggered tissues, we identified RD19 as a prominent $PAD4^{MLF}$ interactor. We found that RD19 also interacts with wild-type PAD4, but not SAG101 or EDS1, and that this interaction is reduced when PAD4 is bound to EDS1. We establish that RD19 and its paralogue RD19c contribute to TNL (RRS1/RPS4)-mediated pathogen restriction and to basal immunity against powdery mildew infection. RD19 has proteolytic activity (Richau *et al.*, 2012) and mutations in the catalytic triad abolished its function in promoting defense responses. We further discovered that whereas PAD4 promotes RD19 maturation and nuclear accumulation, autoimmunity caused by RD19 overexpression is dependent on both EDS1 and PAD4. We propose that PAD4 has an EDS1-independent role assisting RD19 maturation, and that active RD19 creates an EDS1–PAD4-dependent feedback loop to potentiate immune responses.

Materials and methods

Plant materials, growth conditions, and pathogen strains

Arabidopsis accession Col-0 was used in all experiments. The *eds1-2* (Bartsch *et al.*, 2006), *pad4-1* (Jirage *et al.*, 1999), *sag101-3* (Cui *et al.*, 2018), and *pad4 sag101* (Cui *et al.*, 2018) mutants have been published. Arabidopsis mutants *rd19* and *rd19c* were obtained from The Arabidopsis Information Resource (TAIR, Stanford, CA, USA). The *rd19 rd19c* double mutant was generated by crossing *rd19* with *rd19c*. *RD19* overexpression (OE-RD19, 35S:RD19-Flag), $RD19^{C159A}$ overexpression (OE-$RD19^{C159A}$, 35S:$RD19^{C159A}$-FLAG), and $RD19^{N329A}$ overexpression (OE-$RD19^{N326A}$, 35S:$RD19^{N326A}$-FLAG) transgenic lines were generated using the floral-dip method (Clough and Bent, 1998). The *RD19* overexpression in *eds1-2* was generated by crossing OE-RD19 line #2 with *eds1-2*. The *RD19* overexpression lines in *pad4-1*, *sag101-3*, or *pad4-1 sag101-3* were generated by crossing OE-RD19 line #2 with *pad4-1 sag101-3*. *Pseudomonas syringae* pv. *tomato* (*Pst*) strain DC3000 and *Pst* DC3000 *AvrRps4* were maintained as previously described (Cui *et al.*, 2018). The seeds were germinated on Murashige and Skoog (MS) medium plates and then transplanted into soil after 10 d. All plants were grown in a growth chamber at 22 °C and 65% relative humidity, with 9 h/15 h (light/dark) period and a light intensity of 150 μmol m^{-2} s^{-1}.

Golden gate cloning and generation of Arabidopsis transgenic lines

The coding sequence of *RD19* and *RD19C* without a stop codon was amplified from Col-0 cDNA and cloned into Level (L) 0 vector pAGM1287. The genes were then cloned into L1 vector pICH47811 and L2 vector pICH86966 (with kanamycin resistance as selection marker in the transgenic plants) to fuse it with a CaMV 35S promoter and C-terminal 3× FLAG tag. The backbones, 35S promoter (pICH51266) and terminator (pICH41414) modules were from the Golden Gate cloning toolkit (Addgene, Waterown, MA USA) (Engler *et al.*, 2014). The primers used for cloning are provided in Supplementary Table S1. The L2 construct of *RD19-FLAG* was transformed into *Agrobacterium* GV3101, and transgenic lines were generated by *Agrobacterium*-mediated floral dipping of Col-0 plants.

Pathogen infection assays

For pathogens growth assays, *Pst* DC3000 or *Pst* DC3000 *AvrRps4* was cultured overnight in KB medium at 28 °C in a 200 rpm shaker, and the cultured cells were collected by centrifuging at 4000 rpm. The bacteria then were diluted at OD_{600}=0.2 in water plus 0.02% Silwet-77 for spray infection on 4-week-old Arabidopsis leaves. Bacterial titers were measured at 3 days post-infection (dpi) as described (Feys *et al.*, 2005). Statistical analysis on bacterial growth data from three or two independent experiments with six biological replicates in each experiment (as indicated in the figure legends) was determined by one-way ANOVA followed by Tukey's honestly significant difference (HSD) test.

For powdery mildew infection, spores of *Golovinomyces cichoracearum* strain UCSC1 maintaining on *pad4-1* leaves were blown onto the plants to be infected. The infected leaves were stained with trypan blue at 5 dpi to visualize hyphae and quantify the number of conidiophores per colony (Frye and Innes, 1998).

Hyaloperonospora arabidopsidis (*Hpa*) isolate Emwa1 was spray-inoculated on 4.5-week-old plants with a spore concentration of 4×10^4 spores ml^{-1} and trypan blue staining was performed at 4 dpi, to visualize both cell death and free hyphae growth by light microscopy. Spores were counted at 7 dpi and the number of spores was normalized to the corresponding plant fresh weight. Statistical analysis of spore counts from three biological replicates, consisting of two technical replicates (pool of four to six plants each) was performed by ANOVA (data transformation using quadratic root to reach a normal distribution of the data) with multiple comparison using Tukey's HSD test.

Quantitative reverse transcription–PCR assay

Total plant RNA was extracted with TRIzol Regent (Thermo Fisher Scientific, cat. no. 15596018), and then cDNA was obtained using GoScriptTM Reverse Transcription kit (Promega, cat. no. M1708). Quantitative reverse transcription–PCR (qRT–PCR) assays were performed on a CFX Connect machine (Bio-Rad Laboratories). Expression of the test genes was normalized to *AT4G26410* (Cui *et al.*, 2018). The primers used for qRT–PCR are provided in Supplementary Table S1.

Transient expression in Arabidopsis protoplasts

Arabidopsis protoplasts and transfections were performed as described (Li *et al.*, 2005). Transfected protoplasts were incubated at room temperature under weak light (1.5 μmol m^{-2} s^{-1}) for 12~16 h for expressing target proteins.

Trypan blue staining

Arabidopsis leaves were stained with trypan blue according to Koch and Slusarenko (1990) and observed with ×10 magnification under a Zeiss Axiocam 506 color light microscope.

Protein extraction, immunoprecipitation, and immunoblotting

These experiments were performed as described (Cui *et al.*, 2018). Antibodies used were anti-green fluorescent protein (GFP; Transgen, cat. no. HT801), anti-FLAG (Abcam, cat. no. ab49763), anti-hemagglutinin (HA) (Roche, cat. no. 11867423001), anti-mouse IgG (Abbkine, cat. no. A21010), anti-rat IgG (Earthox, cat. no. E030140), and anti-rabbit IgG (Abbkine, cat. no. A21020).

Split-luciferase complementation assay

A split-luciferase complementation assay was performed as described (Chen *et al*., 2008). *Agrobacterium tumefaciens* (GV3101 PM90) carrying the indicated nLUC and cLUC constructs was mixed and infiltrated into the leaves of *N. benthamiana* using a needle-less syringe. Two days post-infiltration, the leaves were rubbed with 1 mM luciferin and kept in the dark for 5 min to quench the fluorescence. Then the luciferase images were captured with a cooled CCD imaging apparatus (Berthold, cat. no. LB985).

Results

A functional PAD4 variant interacts weakly with EDS1

We reported previously that simultaneous exchanges of amino acids (M16A, L21S, F143A) in the N-terminal lipase domain of Arabidopsis PAD4 (PAD4^{MLF}) strongly reduced its association with EDS1 and thus EDS1–PAD4 dimer formation (Wagner *et al*., 2013). To test whether this mutation impairs immunity, transgenic lines expressing *PAD4^{MLF}* or *PAD4* under the native promoter were generated in an Arabidopsis *pad4-1 sag101-3* double mutant background. Immunoblotting assays showed that the *PAD4^{MLF}* lines accumulated much less PAD4 protein than the *PAD4* lines (Fig. 1A), suggesting that PAD4^{MLF} protein is less stable than wild type (WT) PAD4. This finding is in line with PAD4 stabilization as a dimer with EDS1 (Feys *et al*., 2005; Wagner *et al*., 2013). We tested pathogen resistance of these transgenic lines to the avirulent bacterial strain *Pseudomonas syringae* pv *tomato* DC3000 expressing the effector protein AvrRps4 (*Pst AvrRps4*), which, in addition to PopP2, is recognized by the TNL pair RRS1/RPS4 conferring ETI (Le Roux *et al*., 2015; Sarris *et al*., 2015). Unexpectedly, *PAD4^{MLF} pad4-1 sag101-3* lines restricted *Pst AvrRps4* growth as efficiently as *PAD4 pad4-1 sag101-3* and wild type (WT, Col-0) or *sag101-3* (Fig. 1B). This indicated that *PAD4^{MLF}* fully complements *pad4 sag101* in RRS1/RPS4-triggered immunity. These results suggest that although PAD4^{MLF} is impaired in its interaction with EDS1 and accumulates to low levels, it is still able to mediate TNL RRS1/RPS4 signaling leading to pathogen restriction in ETI.

We tested whether PAD4^{MLF} requires *EDS1* to confer immunity by transforming *YFP*-fused *PAD4^{MLF}* under control of a constitutive CaMV 35S promoter into the *pad4-1* single or *pad4-1 eds1-2* double mutant. Two independent transgenic lines accumulating similar levels of PAD4^{MLF} protein in each background were selected (Fig. 1C). In *Pst AvrRps4* growth assays, the *PAD4^{MLF}-YFP pad4-1* lines were as resistant as WT Col-0 plants (Fig. 1D) indicating that PAD4^{MLF}–yellow fluorescent protein (YFP) complements *pad4-1* in TNL RRS1/RPS4 ETI. By contrast, *PAD4^{MLF}-YFP pad4-1 eds1-2* lines were as susceptible as *pad4-1 eds1-2* (Fig. 1D). Therefore, *EDS1* is required for PAD4^{MLF} signaling in ETI even though EDS1 association with PAD4^{MLF} is impaired.

The requirement of EDS1 for PAD4^{MLF} activity prompted us to re-evaluate the interaction between the two proteins. In co-immunoprecipitation (Co-IP) assays after transient expression in Arabidopsis Col-0 protoplasts, we found that very low amounts of HA-tagged EDS1 co-purified with PAD4^{MLF}–YFP compared with PAD4–YFP (Fig. 1E), indicating that PAD^{MLF} interacts weakly with EDS1. Therefore, we reasoned that weak association between PAD4^{MLF} and EDS1, likely conferred by their C-terminal 'EP' domain interfaces (Wagner *et al*., 2013), is sufficient for TNL-mediated ETI.

RD19 specifically interacts with PAD4 but not SAG101 or EDS1

Because PAD4^{MLF} is less tightly bound by EDS1, we reasoned that PAD4^{MLF} might be a useful bait to identify further co-functioning immunity components. We therefore expressed PAD4^{MLF}–YFP or YFP (as control) in Arabidopsis *pad4-1* protoplasts for immunoprecipitation (IP) experiments. PAD4^{MLF}–YFP and YFP were purified on GFP-trap beads and the eluted proteins analysed using liquid chromatography followed by tandem mass spectrometry (LC–MS/MS). Compared with the YFP control, PAD4^{MLF}–YFP-enriched proteins were identified. One of these was EDS1 (Supplementary Fig. S1A; Supplementary Table S2), further supporting the weak association between EDS1 and PAD4^{MLF}. The papain-like cysteine protease RD19 (AT4G39090) was found among the PAD4^{MLF}-associated proteins (Supplementary Fig. S1A; Supplementary Table S2). Notably, RD19 was also identified as a significant IP–MS/MS interactor of YFP–PAD4 in Arabidopsis leaves after pathogen activation of TNL RRS1/RPS4 ETI (Sun *et al*., 2021). We confirmed that RD19 fused to a FLAG tag (RD19–FLAG) co-purified with both PAD4–YFP and PAD4^{MLF}–YFP in Arabidopsis *pad4-1* protoplast transient assays (Fig. 2A). RD19–FLAG did not interact with EDS1–YFP or SAG101–YFP in IP assays (Fig. 2B). Interestingly, two bands of RD19–FLAG were detected in the PAD4 IP samples, but only one band in the input samples (Fig. 2A, B). Papain-like cysteine proteases usually have an auto-inhibitory domain that is removed during the protease maturation (van der Hoorn, 2008). The second band of RD19–FLAG in the IP samples might be a processed form of RD19 that was enriched by interacting with PAD4. Split-luciferase transient expression assays in *N. benthamiana* further indicated that RD19 interacts preferentially with PAD4 and not with EDS1 or SAG101 (Fig. 2C). We concluded from these data that there is a stable association between PAD4 and RD19 in both non-triggered and immune-triggered cells.

We next tested whether RD19 interacts with PAD4 when it is bound to EDS1 in the heterodimer. For this, RD19–FLAG and PAD4–YFP were co-expressed with or without EDS1–HA in *eds1-2* protoplasts and the proteins immunoprecipitated using GFP-trap beads. In the presence of EDS1–HA, which forms a stable dimer with PAD4, lower amounts of RD19–FLAG protein co-purified with PAD4–YFP (Fig. 2D). Consistent with EDS1 interacting weakly with PAD4^{MLF},

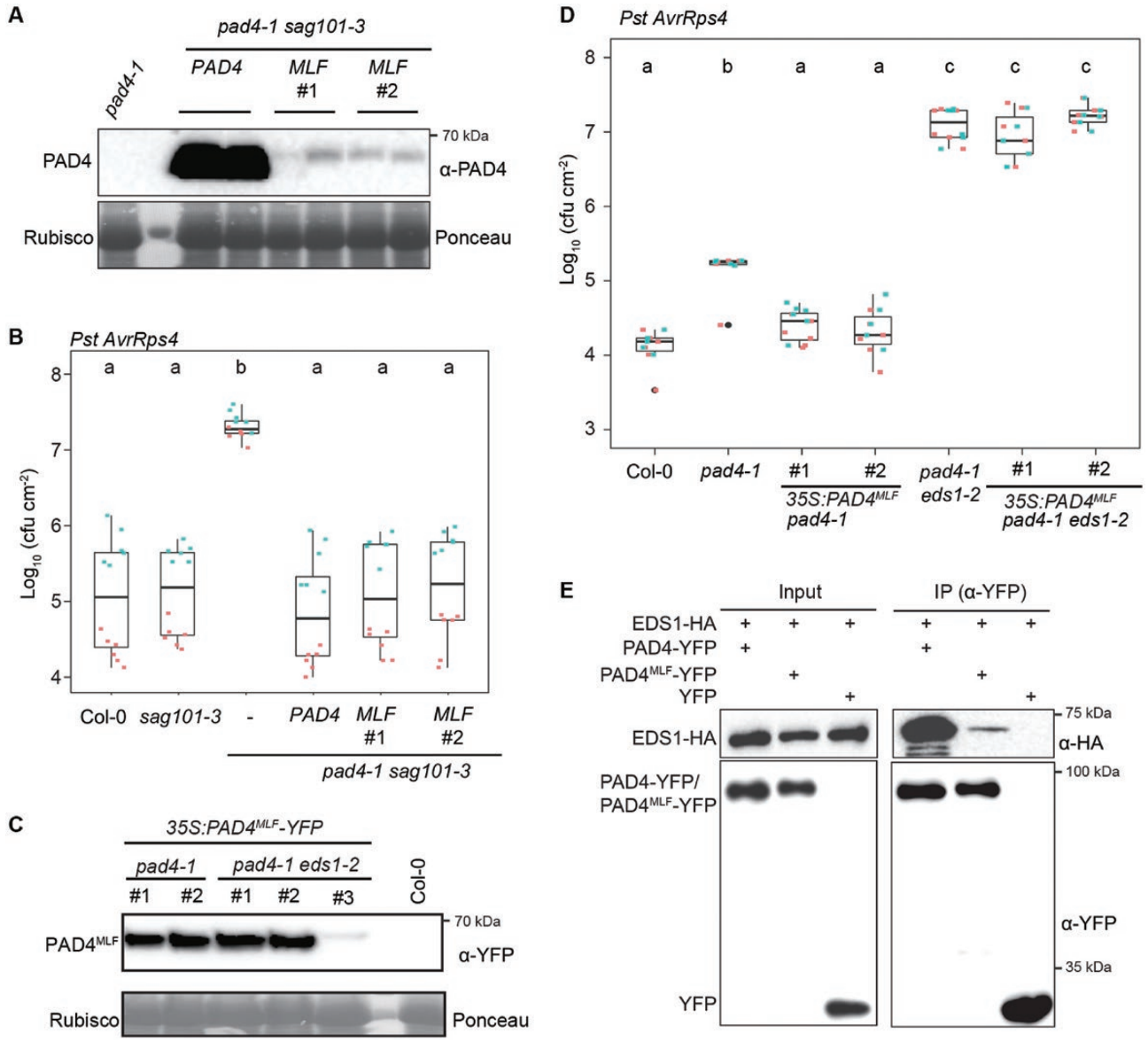

Fig. 1. A functional PAD4^{MLF} variant interacts weakly with EDS1. (A) Immunoblot probed with anti-PAD4 antibody showing PAD4 protein accumulation in transgenic Arabidopsis lines expressing *PAD4* or *PAD4^{MLF}* (MLF #1, MLF #2) under its native promoter in the *pad4-1 sag101-3* mutant background, with the *pad4-1* mutant as a negative control. Ponceau staining of the blots indicates equal loading. (B) Growth of *Pseudomonas syringae* pv. *tomato* DC3000 expressing the effector AvrRps4 (*Pst AvrRps4*) on lines from (A) with WT Col-0 and *sag101-3* mutant as control. Leaves of 4-week-old plants were infiltrated with bacterial suspensions (OD_{600}=0.0002), and bacterial titers were determined at 3 days post-infection (dpi). Dots with different colors in boxplots represent two independent experiments with six biological replicates in each experiment. Different letters indicate statistical significance (P<0.01) determined by one-way ANOVA followed by Tukey's HSD. (C) Immunoblot probed with anti-yellow fluorescent protein (YFP) antibody showing PAD4 protein accumulation in transgenic Arabidopsis lines expressing *PAD4^{MLF}-YFP* under the CaMV *35S* promoter in the *pad4-1* or *pad4-1 eds1-2* mutant background, with WT Col-0 as the negative control. Ponceau staining of the blots indicates equal loading. (D) Growth of *Pst AvrRps4* on lines from (C) with WT Col-0, *pad4-1* and *pad4-1 eds1-2* mutant as a control. Leaves of 4-week-old plants were infiltrated with bacterial suspensions (OD_{600}=0.0002), and bacterial titers were determined at 3 dpi. Dots with different colors in boxplots represent two independent experiments with six biological replicates in each experiment. Different letters indicate statistical significance (P<0.01), as determined by one-way ANOVA followed by Tukey's HSD test. (E) Co-immunoprecipitation analysis of the interaction between EDS1–HA and PAD4–YFP or PAD4^{MLF}–YFP in transfected Arabidopsis *eds1-2* protoplasts. Proteins in total extracts (input) and after immunoprecipitation (IP) with GFP-trap beads [IP (anti (α)-YFP)] were detected on immunoblots using α-HA or α-GFP antibodies. The experiment was repeated three times with consistent results.

EDS1 did not compete with RD19 for PAD4^{MLF} interaction (Fig. 2D). Taken together, the data suggest that EDS1 bound to PAD4 limits PAD4–RD19 association.

Since RD19 interacts with PAD4 or PAD4^{MLF}, we investigated which domain of PAD4 is responsible for the association. When expressed alone, the C-terminal EP-domain portion of

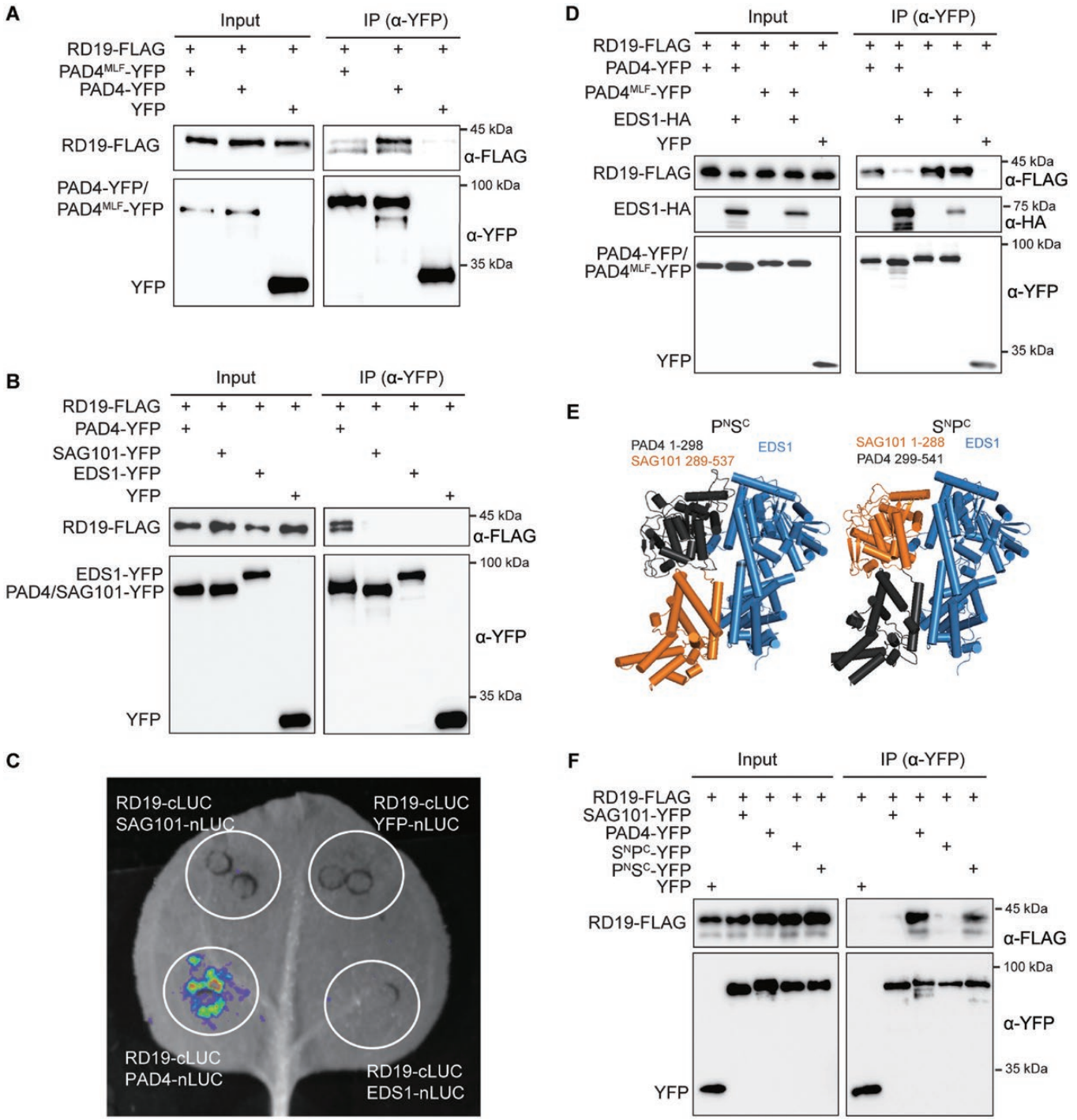

Fig. 2. RD19 specifically interacts with PAD4 but not with EDS1 or SAG101. (A) Co-IP analysis of the interaction between RD19–FLAG and PAD4–YFP or PAD4^{MLF}–YFP in transfected Arabidopsis Col-0 protoplasts. Proteins in total extracts (input) and after IP with anti-GFP beads [IP (α-YFP)] were detected on immunoblots using α-FLAG or α-GFP antibodies. (B) Co-IP analysis of the interaction between RD19–FLAG and EDS1–YFP, PAD4–YFP, or SAG101–YFP in transfected Arabidopsis Col-0 protoplasts. Proteins in total extracts (input) and after IP with anti-GFP beads [IP (α-YFP)] were detected on immunoblots using α-FLAG or α-GFP antibodies. (C) Split-luciferase assays of the interaction between RD19–cLUC and EDS1–nLUC, PAD4–nLUC, SAG101–nLUC, or YFP–nLUC in *N. benthamiana* leaves. Luciferase complementation imaging assays were performed 2 d after co-infiltration of *Agrobacterium* expressing indicated plasmids. (D) Co-IP analysis of the interaction between RD19–FLAG and PAD4–YFP or PAD4^{MLF}–YFP with or without co-expression of EDS1–HA in transfected Arabidopsis *pad4-1* protoplasts. Proteins in total extracts (input) and after IP with anti-GFP beads [IP (α-YFP)] were detected on immunoblots using α-FLAG, α-HA, or α-GFP antibodies. (E) Schematic representation of the PAD4–SAG101 chimeras used in the Co-IP assay shown in (E). The EDS1–SAG101 crystal structure (PDB ID 4nfu) is used as background with PAD4 or SAG101 portions and amino

acid positions shown in brown and green, respectively. EDS1 is shown in blue. (F) Co-IP analysis of the interaction between RD19–FLAG and PAD4–YFP, SAG101–YFP, chimeric protein S^NP^C–YFP ($SAG101^{1–288}PAD4^{299–541}$–YFP) or P^NS^C–YFP ($PAD4^{1–298}SAG101^{289–537}$–YFP) in transfected Arabidopsis Col-0 protoplasts. Proteins in total extracts (input) and after IP with anti-GFP beads [IP (α-YFP)] were detected on immunoblots using α-FLAG or α-GFP antibodies. These experiments were repeated three times with consistent results.

PAD4 is unstable (Supplementary Fig. S1B) (Wagner *et al.*, 2013). We therefore generated two chimeric proteins using the EDS1–SAG101 dimer structure as guide (Wagner *et al.*, 2013; Lapin *et al.*, 2019): an N-terminal PAD4 lipase-like domain ($PAD4^{LLD}$) fused with a C-terminal SAG101 EP-domain (P^NS^C, $PAD4^{1-298}SAG101^{289-537}$) and N-terminal SAG101 fused with C-terminal PAD4 (S^NP^C, $SAG101^{1-288}PAD4^{299-541}$) (Fig. 2E). In Arabidopsis *pad4-1* protoplast assays, RD19–FLAG co-purified with YFP–P^NS^C but not with YFP–S^NP^C (Fig. 2F). This indicates that the PAD4 N-terminal lipase-like domain determines specific interaction with RD19. Furthermore, in *in vitro* pull-down experiments showed that His-tagged $PAD4^{LLD}$ co-purified with glutathione *S*-transferase (GST)-tagged RD19 when expressed in *Escherichia coli* (Supplementary Fig. S1C). Together, the results suggest that PAD4 associates directly with RD19 via the PAD4 N-terminal lipase-like domain and that this association does not require PAD4's direct signaling partner, EDS1, or an immunity trigger.

RD19 and paralog RD19C positively regulate RRS1/RPS4 ETI to bacteria and basal immunity to powdery mildew

A protein BLAST and phylogenetic tree analysis revealed that RD19 has two close homologs, RD19B (AT2G21430) and RD19C (AT4G16190), in the Arabidopsis genome (Supplementary Fig. S2A) (Richau *et al.*, 2012). Expression of *RD19* and *RD19C*, but not *RD19B*, was increased in Arabidopsis RPS4/RRS1-mediated ETI to *Pst AvrRps4* (Supplementary Fig. S2B). Similar *RD19*- and *RD19C*-induced expression trends were observed in a 28 °C→19 °C temperature shift-induced *RPS4* autoimmune line (Heidrich *et al.*, 2013), while *RD19B* expression was barely detected (Supplementary Fig. S2C). These data suggest that *RD19* and *RD19C* might contribute to TNL immunity. In Arabidopsis protoplast IP assays, RD19C also associated with PAD4 but not with EDS1 or SAG101 (Supplementary Fig. S2D).

We obtained T-DNA insertion mutants of *rd19* (Salk_031088) and *rd19c* (SAIL_355_D07) from the Arabidopsis Biological Resource Center (ABRC). Homozygosity of the T-DNA inserts was verified in selected mutant lines by PCR (Supplementary Fig. S2E). To test for possible redundancy between *RD19* and *RD19C*, we generated an *rd19 rd19c* double mutant by crossing *rd19* with *rd19c*. Using the mutants, we measured the contribution of RD19 and RD19C to RRS1/RPS4-mediated resistance to *Pst AvrRps4* after spray inoculation of bacteria onto leaves. Bacterial growth in leaves was slightly increased in *rd19* or *rd19c* single mutants and was further increased in the *rd19 rd19c* double mutant (Fig. 3A). These data suggest that RD19 and RD19C contribute positively to RRS1/RPS4 TNL ETI in a partially redundant manner.

To test whether RD19 and/or RD19C promote TNL ETI against a different pathogen, we inoculated plants with the oomycete *Hyaloperonospora arabidopsidis* (*Hpa*) isolate Emwa1, which is recognized by TNL RPP4 in Col-0 (van der Biezen *et al.*, 2002). In this response, *rd19*, *rd19c*, and *rd19 rd19c* double mutants displayed similar levels of resistance to WT and all produced a hypersensitive response with no *Hpa* sporulation (Supplementary Fig. S3A, B). We concluded that RD19 and RD19C have a minor or no impact on RPP4-mediated resistance to *Hpa*.

We further investigated *RD19* and *RD19C* involvement in EDS1/PAD4-mediated basal resistance to virulent pathogen strains. Bacterial growth assays with virulent *Pst* DC3000 showed that *rd19*, *rd19c*, and *rd19 rd19c* mutants were no more susceptible than WT Col-0 plants (Supplementary Fig. S3C). Therefore, *RD19* and *RD19C* are dispensable for basal immunity to *Pst* DC3000. By contrast, inoculations with virulent powdery mildew isolate *Golovinomyces cichoracearum* revealed more severe disease symptoms (Fig. 3B) and higher sporulation (Fig. 3C) on leaves of *rd19*, *rd19c*, and *rd19 rd19c* than on WT Col-0. Therefore, *RD19* and *RD19C* have positive roles in basal resistance to powdery mildew infection. We concluded that genetic contributions of *RD19* and its paralog *RD19C* coincide with only a subset of *PAD4*-dependent TNL ETI and basal immunity in Arabidopsis.

RD19 *overexpression leads to autoimmunity*

To further explore the role of RD19 in plant immunity, Arabidopsis lines expressing *RD19-FLAG* driven by the constitutive 35S promoter were generated in WT Col-0. Two independent homozygous lines accumulating different levels of RD19–FLAG protein were selected (OE-RD19 #1, #2) (Fig. 4A). We noticed that 4-week-old OE-RD19 #2 plants with highest RD19 protein accumulation were smaller than OE-RD19 #1 and WT plants (Fig. 4B). Five-week-old plants of both OE-RD19 #1 and #2 lines exhibited early leaf senescence (Fig. 4B). Staining of leaf cells with trypan blue revealed that OE-RD19 #2 started to show spontaneous cell death at 4 weeks (Fig. 4C). Similarly, cell death was detected in OE-RD19 #1 plants at 5 weeks (Fig. 4C). Thus, overexpression of *RD19* leads to protein dosage- and age-dependent spontaneous cell death.

We measured resistance of 4-week-old OE-RD19 plants to virulent pathogens. Inoculated *Pst* DC3000 bacteria reached

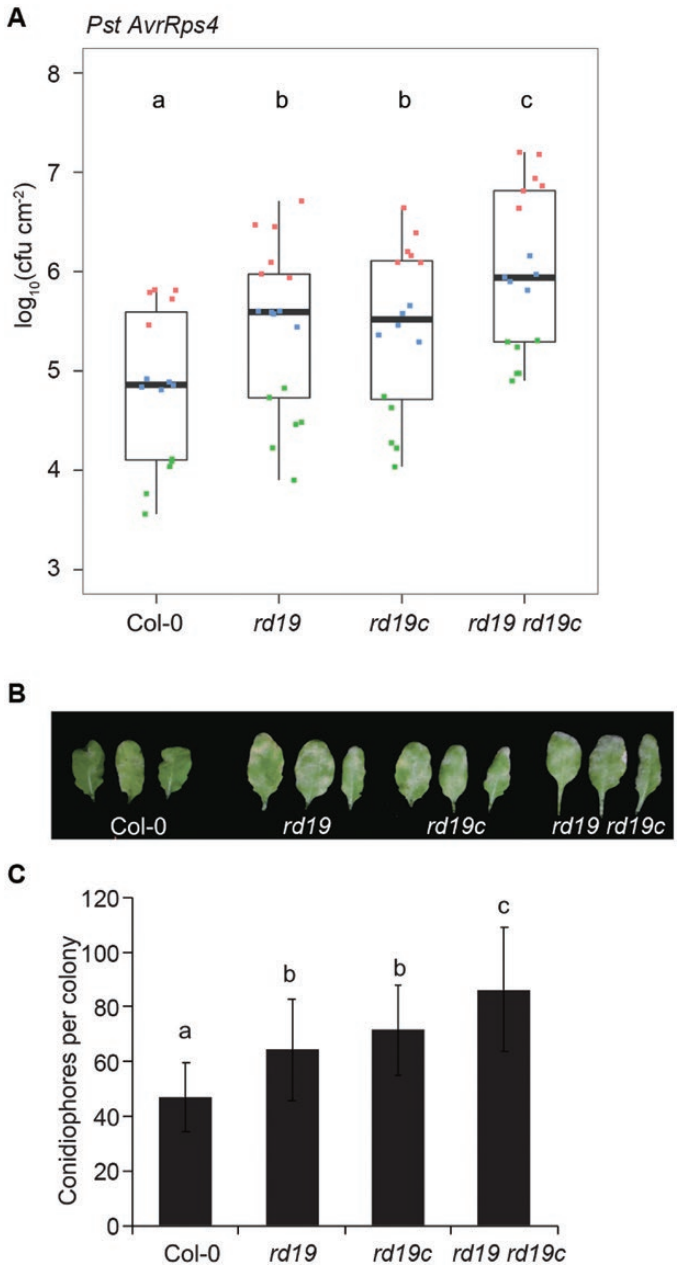

Fig. 3. RD19 and RD19C positively regulate RRS1/RPS4-mediated ETI and basal defense to powdery mildew. (A) Growth of *Pst* DC3000 *AvrRps4* in leaves of Col-0, *rd19*, *rd19c*, and *rd19 rd19c*. Leaves of 4-week-old plants were spray infected with bacterial suspensions (OD_{600}=0.2), and bacterial titers were determined at 3 days post-infection (dpi). Dots with different colors in boxplots represent three independent experiments with six biological replicates in each experiment. Different letters indicate statistical significance (P<0.01) determined by one-way ANOVA followed by Tukey's HSD test. (B) Powdery mildew symptoms on leaves of Arabidopsis plants at 9 dpi with *Golovinomyces cichoracearum*. (C) Quantification of fungal growth in plants at 5 dpi by counting the number of conidiophores per colony. Bars represent mean ±SD (n≥20). Letters indicate significant differences (P<0.05; one-way ANOVA). The experiment was repeated three times with similar results.

10-fold lower titers on OE-RD19 #1 and ~100-fold less on OE-RD19 #2 plants than on WT Col-0 (Fig. 4D). Therefore, *RD19* overexpression enhances basal immunity to *Pst* DC3000. qRT–PCR assays showed that expression of the *PR1* and salicylic acid (SA) synthesis *ICS1* defense marker genes was constitutively high in OE-RD19 plants compared with WT Col-0, which showed induced defense gene expression in response to *Pst* DC3000 (Fig. 4E). Across assays, the extent of plant growth retardation, spontaneous cell death, bacterial resistance, and constitutive expression of defense genes in the OE-RD19 lines correlated with RD19 protein levels (Fig. 4). The OE-RD19 plants were also more resistant to powdery mildew (*G. cichoracearum*) infection. Plants displayed extensive lesioning (Fig. 4F) and fewer conidiophores per colony in leaves at 5 dpi (Fig. 4G). These results show that overexpression of *RD19* in Arabidopsis results in autoimmunity and enhanced resistance to virulent pathogens.

Protease activity of RD19 is required for its immunity promotion

RD19 encodes a papain-like cysteine protease in subfamily C1A with measurable proteolytic activity (Richau *et al.*, 2012). As a C1A protease, RD19 is predicated to have a signal peptide that likely targets the protein to the vacuole (Bernoux *et al.*, 2008), an autoinhibitory pro-domain, and a protease enzymatic domain with a catalytic triad of Cys^{159}, His^{302}, and Asn^{329} for auto-processing and cleavage of potential target substrates (https://www.uniprot.org) (Fig. 5A). C1A proteases are normally produced as prepro-proteases (the full length protein containing signal peptide, pro-domain, and protease domain) in which the autoinhibitory pro-domain is removed during activation of the protease (van der Hoorn, 2008). When examining accumulation of RD19–FLAG protein in *OE-RD19* lines by immunoblotting, we detected two RD19–FLAG specific bands of ~ 44 kDa and 41 kDa (Fig. 4A; Supplementary Fig. S4A) that we predicted to correspond, respectively, to the prepro-protease and pro-protease (pro plus protease domain) forms of RD19 with the FLAG epitope tag.

To test whether RD19 promotes immunity through its protease activity, we generated transgenic Arabidopsis lines expressing *RD19*^{C159A}*-FLAG* or *RD19*^{N329A}*-FLAG* mutations in the predicted catalytic site residues, also driven by the CaMV 35S promoter. Two independent OE-$RD19^{N329A}$ and OE-$RD19^{C159A}$ homozygous lines (#1 and #2) with similar RD19 transcript and protein levels as OE-RD19 lines #1 and #2 were selected (Fig. 5B; Supplementary Fig. S4B). On immunoblots, the RD19 lower band (likely corresponding to the pro-protease form of RD19) was much weaker in the OE-$RD19^{N329A}$ and OE-$RD19^{C159A}$ mutants compared with OE-RD19 WT proteins (Fig. 5B). We interpreted this as correlating with RD19 auto-proteolytic activity in RD19

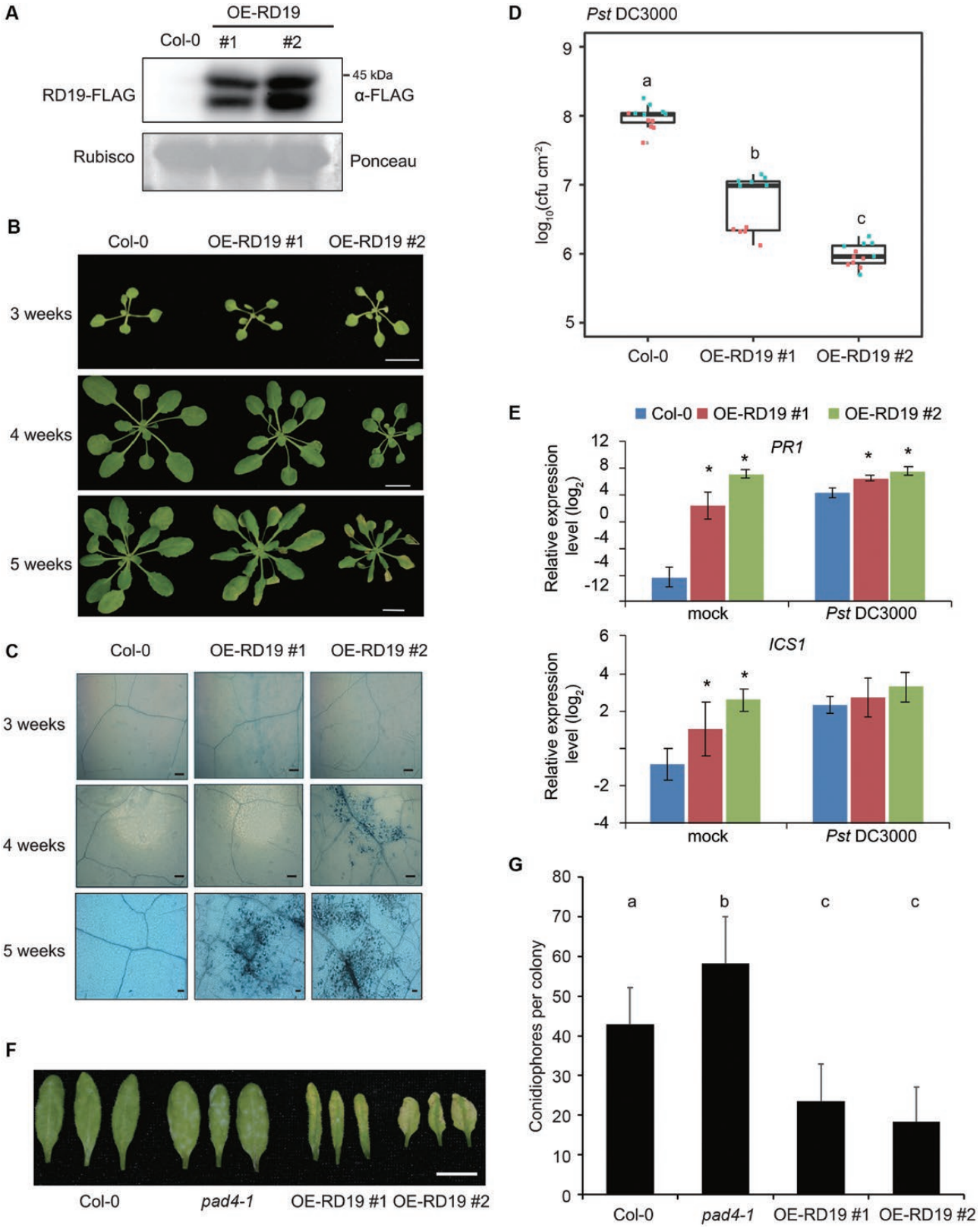

Fig. 4. Overexpression of *RD19* results in autoimmunity and enhances resistance to virulent pathogens. (A) Immunoblot probed with anti-FLAG antibody showing RD19–FLAG protein accumulation in transgenic Arabidopsis lines expressing *RD19-FLAG* (OE-RD19 #1, #2) under the 35S promoter in the Col-0 background, with WT Col-0 as the negative control. Ponceau staining of the blots indicates equal loading. (B) Developmental phenotype of 3-,

4-, and 5-week-old plants of transgenic lines in (A). Scale bars: 1 cm. (C) Trypan blue staining of cell death in leaves of plants in (B). Scale bars: 1 mm. (D) Growth of *Pst* DC3000 in leaves of Col-0, OE-RD19 #1 and #2. Leaves of 4-week-old plants were spray infiltrated with bacterial suspensions (OD_{600}=0.2), and bacterial titers were determined at 3 days post-infection (dpi). Dots with different colors in boxplots represent two independent experiments with six biological replicates in each experiment. Different letters indicate statistical significance (P<0.01), as determined by one-way ANOVA followed by Tukey's HSD test. (E) Expression of the salicylic acid pathway genes *PR1* and *ICS1* in Col-0 and OE-RD19 #1 and #2 measured by qRT–PCR. Gene expression was normalized to *AT4G26410*. Error bars represent the mean ±SD of three biological replicates. Significant difference from Col-0 using Student's *t*-test: *P<0.05. (F) Powdery mildew symptoms on leaves of Col-0, *pad4-1*, OE-RD19 #1 and #2 at 8 dpi with *G. cichoracearum*. Scale bar: 1 cm. (G) Quantification of fungal growth on Col-0, *pad4-1*, OE-RD19 #1 and #2 plants at 5 dpi by counting the number of conidiophores per colony. Bars represent mean ±SD (n≥20). Letters indicate significant differences (P<0.05; one-way ANOVA). The experiment was repeated three times with similar results.

WT but not in $RD19^{N329A}$ or $RD19^{C159A}$. Also, 5-week-old OE-$RD19^{N329A}$ and OE-$RD19^{C159A}$ plants had no developmental defects or spontaneous cell death (Fig. 5C). Unlike OE-RD19 plants, the OE-$RD19^{N329A}$ and OE-$RD19^{C159A}$ lines had no increased expression of *PR1* and *ICS1* genes (Fig. 5D) and were as susceptible as WT plants to virulent *Pst* DC3000 (Fig. 5E). Put together, these data suggest that RD19 protease activity is required both for its auto-processing and for eliciting an autoimmune response.

RD19-conditioned autoimmunity requires EDS1 *and* PAD4

To dissect the genetic relationship between *RD19* and the *EDS1* family, *RD19-FLAG* overexpression in *eds1-2*, *pad4-1*, *sag101-3*, or *pad4-1 sag101-3* mutant backgrounds was obtained by crossing OE-RD19 line #2 with *eds1-2 or pad4-1 sag101-3*. RD19-FLAG protein levels were examined in the selected mutant lines. Strikingly, the RD19–FLAG lower 41 kDa band (corresponding to pro-protease form of RD19–FLAG) was markedly reduced in *pad4-1* and *pad4-1 sag101-3* but was not affected in a *sag101-3* single mutant (Fig. 6A; Supplementary Fig. S5). Accumulation of pro-RD19-FLAG in *eds1-2* varied between experiments (Fig. 6A; Supplementary Fig. S5). We concluded that PAD4, but not SAG101, promotes accumulation of the pro-RD19 form *in planta*. Also, OE-RD19-mediated stunting was abolished in *eds1-2*, *pad4-1*, or *pad4-1 sag101-3* but not the *sag101-3* mutant (Fig. 6B). qRT–PCR assays showed that *RD19* expression was similar between the different RD19-OE lines and much higher than those expressing endogenous *RD19* (Fig. 6C). OE-RD19 driven constitutive expression of *PR1* and *ICS1* was abolished in the *eds1-2*, *pad4-1*, and *pad4-1 sag101-3* mutants, but not in *sag101-3* (Fig. 6C). Moreover, OE-RD19 in *eds1-2*, *pad4-1*, and *pad4-1 sag101-3* did not enhance resistance to *Pst* DC3000 but did in *sag101-3* (Fig. 6D). These results suggest that while the accumulation of processed RD19 (pro-form) depends mainly on PAD4, OE-RD19-conditioned autoimmunity is both *EDS1*- and *PAD4*-dependent.

PAD4 interacts with the processed RD19 forms

To further clarify whether the processed form of RD19–FLAG detected on blots is the RD19 pro-protease, we generated vectors expressing truncated RD19 forms with C-terminal FLAG tags corresponding to proRD19 without the signal peptide (amino acid 1–22) and $RD19^{134–368}$ lacking signal peptide and pro-domain (amino acids 23–133) (Fig. 7A). The full-length and truncated RD19 proteins were transiently co-expressed with PAD4–YFP or YFP in Arabidopsis protoplasts to validate their molecular masses and test for interactions with PAD4 in a Co-IP assay. As shown in Fig. 7B, proRD19–FLAG (predicted 41.1 kDa with 3×FLAG tag) migrated slightly faster than RD19–FLAG (predicted 43.6 kDa), while the $RD19^{134–368}$–FLAG band (predicted 28.4 kDa) migrated at ~35 kDa on immunoblots (Fig. 7B). This agreed with our prediction that the lower band of RD19–FLAG detected in OE-RD19 plants (Figs 4A, 5B, 6A) likely corresponds to proRD19. Compared to RD19–FLAG, more proRD19–FLAG and $RD19^{134–368}$–FLAG proteins co-purified with PAD4–YFP (Fig. 7B). This finding suggests that PAD4 interacts preferentially with the processed RD19 forms.

PAD4 promotes nuclear accumulation of processed RD19

RD19 has a predicted nuclear localization signal (NLS) at its C-terminus (Supplementary Fig. S6; https://nls-mapper.iab.keio.ac.jp/cgi-bin/NLS_Mapper_form.cgi). We therefore investigated the subcellular localization of RD19 and proRD19. Fully processed $RD19^{134–368}$ was excluded because it was not detected in the OE-RD19 transgenic lines. RD19–YFP and proRD19–YFP were first transiently expressed in *N. benthamiana* leaves. Consistent with previous reports, RD19–YFP was mainly detected in the cytoplasm and in putative mobile vacuole-associated compartments (Fig. 7C) (Bernoux *et al.*, 2008). However, weak RD19–YFP fluorescence was detected within the nucleus, marked by mCherry-tagged histone 3.1 (mCherry–H3.1) (Fig. 7C), suggesting that a small amount of RD19 accumulates in nuclei. By contrast, strong fluorescence of proRD19–YFP was detected in the nucleus (Fig. 7C), suggesting that a major pool of processed RD19 (proRD19) resides in the nucleus.

To test whether proRD19–YFP nuclear localization depends on PAD4, we transiently expressed proRD19–YFP together with the nuclei marker mCherry–H3.1 in Arabidopsis *pad4-1* protoplasts. In these assays proRD19 was observed mainly in the cytoplasm and vesicles but hardly detected in the nucleus

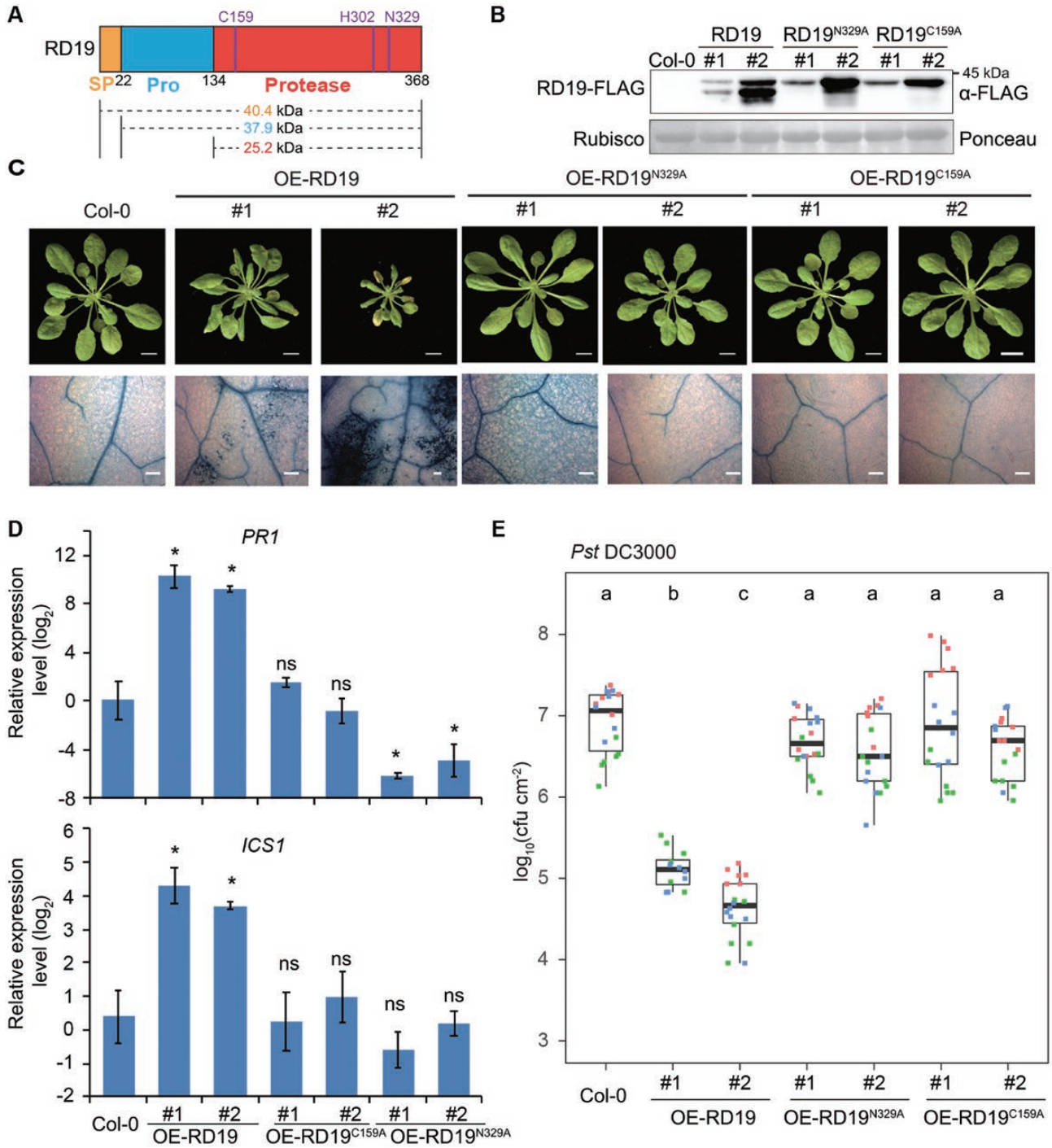

Fig. 5. Protease activity of RD19 is required for its function in immunity. (A) Domains of RD19 are colored. Numbers indicate sites of residues. SP, signal peptide (orange); pro, autoinhibitory prodomain (blue); protease, protease domain (red); C, H, N, catalytic residues Cys, His, and Asn (purple). (B) Immunoblot probed with α-FLAG antibody showing RD19–FLAG, RD19^{N329A}–FLAG, and RD19^{C159A}–FLAG protein accumulation in transgenic Arabidopsis lines expressing FLAG-tagged *RD19* or *RD19* mutants under 35S promoter in the Col-0 background. Ponceau staining of the blots indicates equal loading. (C) Developmental phenotype and trypan blue staining of cell death of 5-week-old transgenic plants in (B). Scale bars: 1 cm (upper panel) or 2 mm (lower panel). (D) Expression of *PR1* and *ICS1* in 5-week-old plants of transgenic lines in (B) measured by qRT–PCR. Gene expression was normalized to *AT4G26410*. Error bars represent the mean ±SD of three biological replicates. Significant difference from Col-0 was determined using Student's *t*-test: **P*<0.05; ns, not significant. (E) Growth of *Pst* DC3000 in leaves of 5-week-old plants of transgenic lines in (B). Leaves of 4-week-old plants were spray infiltrated with bacterial suspensions (OD_{600}=0.2), and bacterial titers were determined at 3 d post-infection. Dots with different colors in boxplots represent three independent experiments with six biological replicates in each experiment. Different letters indicate statistical significance (*P*<0.01), as determined by one-way ANOVA followed by Tukey's HSD test.

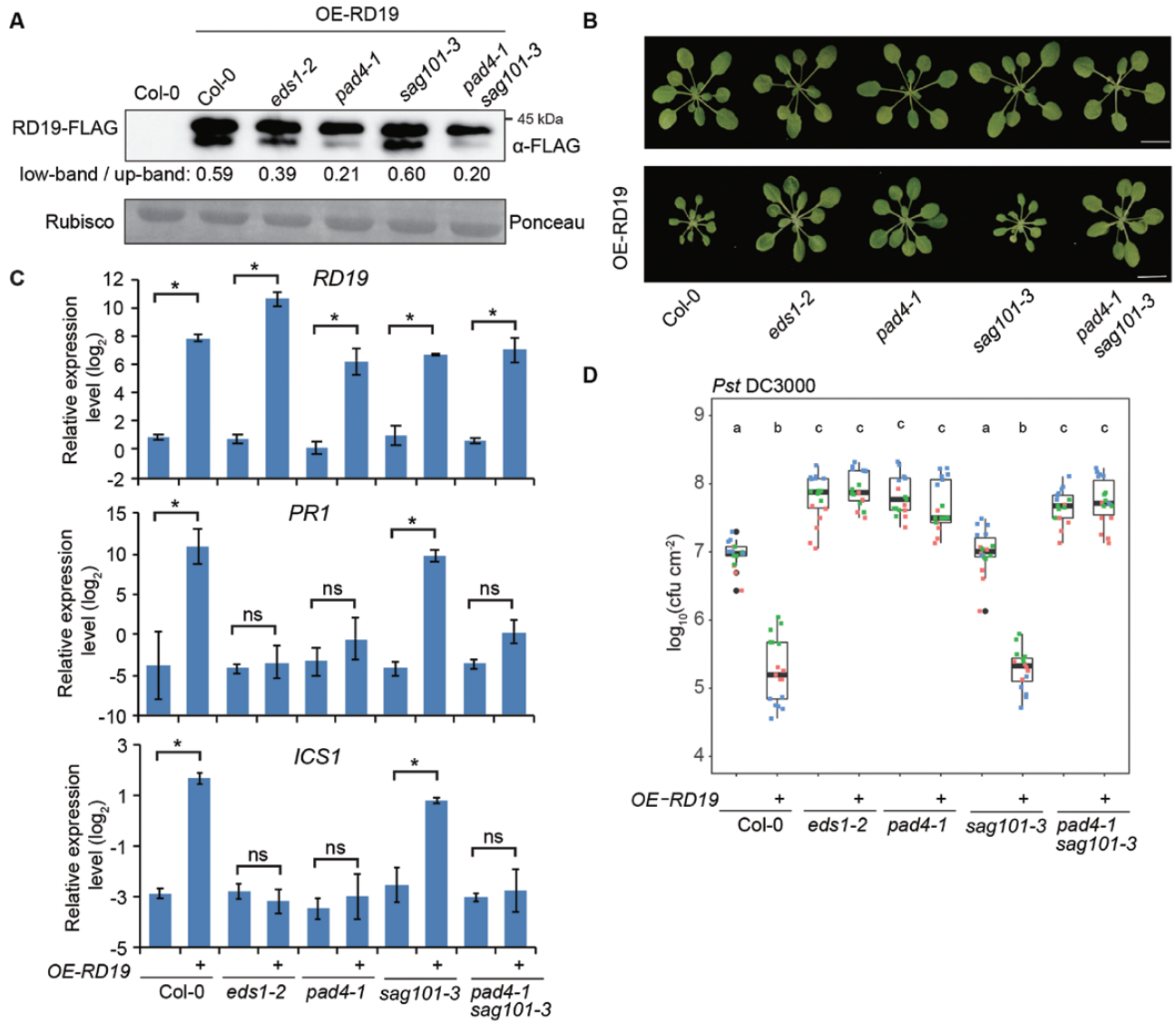

Fig. 6. *EDS1* and *PAD4* are required for *RD19*-mediated autoimmunity. (A) Immunoblot probed with α-FLAG antibody showing RD19–FLAG protein accumulation in the Arabidopsis Col-0, *eds1-2*, *pad4-1*, *pad4-1 sag101-3*, or *sag101-3* background expressing *RD19-FLAG* under the 35S promoter. Ponceau staining of the blots indicates equal loading. (B) Developmental phenotype of 4-week-old Col-0, *eds1-2*, *pad4-1*, *pad4-1 sag101-3*, and *sag101* plants and overexpression of *RD19-FLAG* in each background. Scale bars: 1.5 cm. (C) Expression of the *PR1*, *ICS1*, and *RD19* in 5-week-old plants as indicated in (B) measured by qRT–PCR. Gene expression was normalized to *AT4G26410*. Error bars represent the mean ±SD of three biological replicates. Significant difference from Col-0 or each mutant background was determined using Student's *t*-test: **P*<0.05; ns, not significant. (D) Growth of *Pst* DC3000 in leaves of 5-week-old plants as indicated in (B). Leaves of 4-week-old plants were spray-infiltrated with bacterial suspensions (OD_{600}=0.2), and bacterial titers were determined at 3 d post-infection. Dots with different colors in boxplots represent two independent experiments with six biological replicates in each experiment. Different letters indicate statistical significance (*P*<0.01), as determined by one-way ANOVA followed by Tukey's HSD test.

(Fig. 7D). When co-expressed with PAD4–FLAG, a higher proRD19–YFP nuclear signal was observed (Fig. 7D). This suggests that PAD4 directly or indirectly promotes nuclear accumulation of proRD19–YFP. To test this observation further, we extracted total and nuclear protein fractions from *pad4-1* protoplasts expressing proRD19–YFP alone or together with PAD4–FLAG. Immunoblot assays showed that the proRD19–YFP total and nuclear pools increased in the presence of PAD4–FLAG (Fig. 7E).

Discussion

In Arabidopsis, EDS1 and PAD4 function as a heterodimer to confer TNL immunity as well as basal resistance through their activation of ADR1-family helper NLRs (Sun *et al*., 2021; Wu *et al*., 2021; Huang *et al*., 2022). PAD4 additionally functions independently of EDS1 in reducing infestation by green peach aphid (Pegadaraju *et al*., 2007; Louis *et al*., 2012; Dongus *et al*., 2020). Besides the helper NLRs, other components regulating

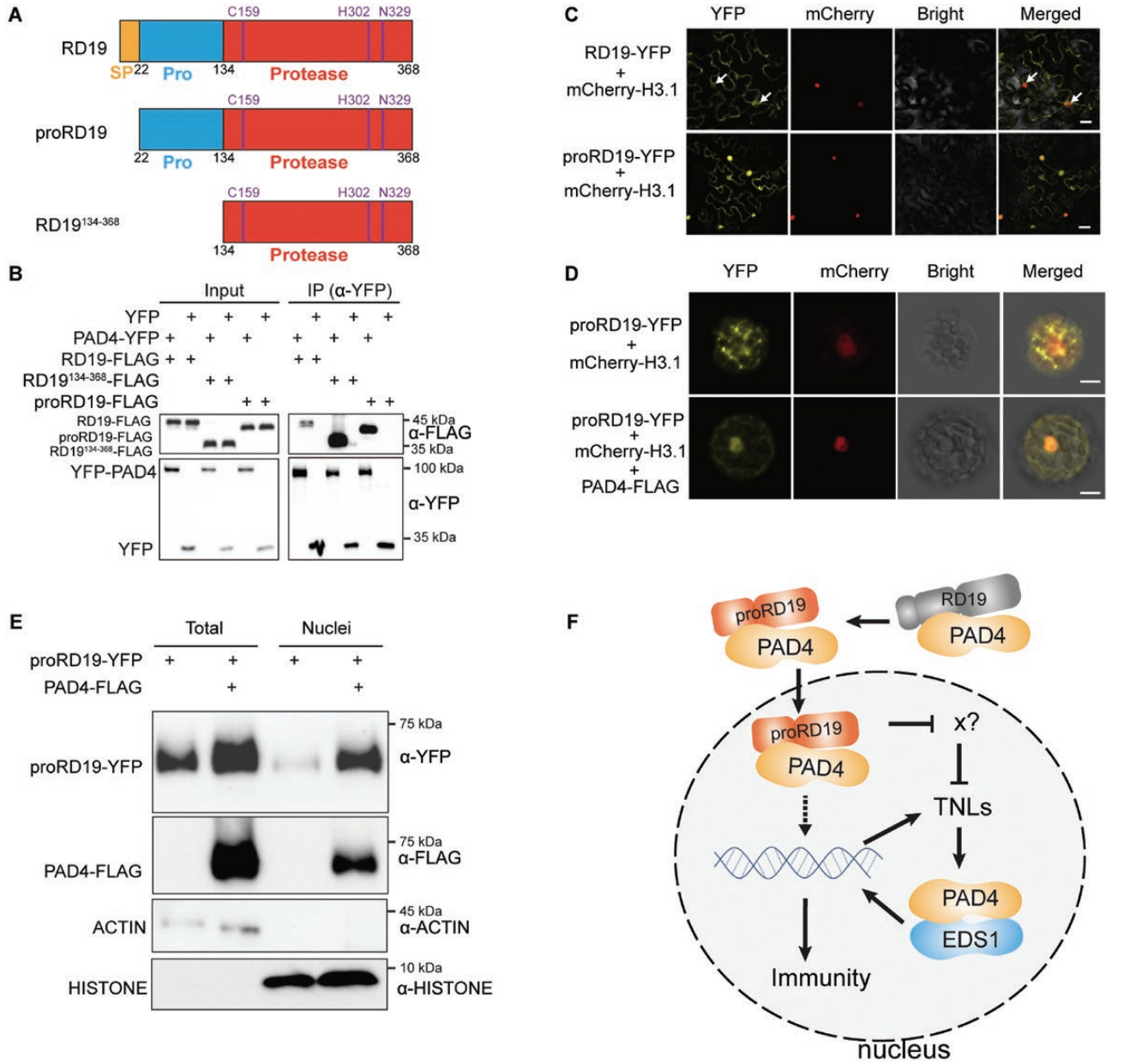

Fig. 7. PAD4 promotes nuclear accumulation of processed RD19. (A) Diagram showing the full-length and truncated versions of RD19. SP, signal peptide; Pro, pro-domain; Protease, protease domain. (B) Co-IP analysis of the interaction between PAD4–YFP and full-length RD19–FLAG or truncated proRD19–FLAG and RD19$^{134–368}$–FLAG in transfected Arabidopsis Col-0 protoplasts. Proteins in total extracts (input) and after IP with α-GFP beads [IP (α-YFP)] were detected on immunoblots using α-FLAG or α-GFP antibodies. (C) Subcellular localization of RD19–YFP and proRD19–YFP in *N. benthamiana.* Confocal images of *N. benthamiana* epidermal cells 2 d after co-expression of a nuclear marker mCherry–histone 3.1 (mCherry–H3.1) with 35S:RD19–YFP or 35S:proRD19–YFP via *Agrobacterium* infiltration. The arrows indicate the nuclei showing weak RD1–YFP fluorescence. Scale bars: 20 μm. (D) ProRD19–YFP alone or together with PAD4–FLAG was co-expressed with mCherry–H3.1 in *pad4-1* protoplasts to visualize the subcellular localization of proRD19–YFP in the cells. In the absence of PAD4, proRD19–YFP was mainly observed in the cytoplasm and mobile vesicles but not in the nucleus. ProRD19–YFP was detected in the nucleus when it was co-expressed with PAD4–FLAG. Scale bars: 10 μm. (E) Detection of proRD19–YFP in the total protein extract and nuclear fraction by immunoblotting. ProRD19–YFP was transiently expressed alone or co-expressed with PAD4–FLAG in *pad4-1* protoplasts for 16 h. Detection of actin and histones by their antibodies indicated successful isolation of nuclei from the protoplasts. (F) A proposed working model for PAD4-regulated RD19 in plant immunity. PAD4 interacts with RD19 and promotes accumulation of processed RD19 (proRD19) in the nucleus, where the activated RD19 might lead to the degradation of negative components and/or up-regulation TIRs or TNLs, resulting in increased production of small molecules that promote EDS1–PAD4 defense. This model does not exclude RD19 proteolytic targeting of multiple immunity components in the cytoplasm, nucleus, and apoplast.

processes downstream of PAD4 have remained elusive. Here, we provide evidence that Arabidopsis papain-like cysteine protease RD19 and its paralog RD19C contribute to some but not all PAD4-regulated immune responses. Our biochemical and genetic evidence shows that RD19 and RD19C specifically interact with PAD4 and help to promote RRS1/RPS4-mediated ETI to bacteria and basal resistance to powdery mildew in leaves (Figs 2, 3). Overexpression of RD19 results in autoimmunity with enhanced resistance to virulent pathogens (Fig. 4), which is fully dependent on RD19 protease activity (Fig. 5). Furthermore, we show that PAD4 influences both RD19 maturation and nuclear accumulation (Figs 6A, 7). The data suggest a molecular and functional link between PAD4 and a cysteine protease in plant immunity.

We previously showed that mutually exclusive EDS1 heterodimers with PAD4 or SAG101 execute distinct functions in Arabidopsis TNL immunity (Rietz *et al*., 2011; Wagner *et al*., 2013; Lapin *et al*., 2019; Dongus *et al*., 2022). EDS1 stable interaction with PAD4 or SAG101 is mediated by a hydrophobic helix in the EDS1 N-terminal lipase-like domain binding to similar N-terminal pockets of PAD4 and SAG101 (Wagner *et al*., 2013). Much weaker interactions were found to be mediated by EDS1–PAD4 and EDS1–SAG101 C-terminal EP-domain interfaces (Wagner *et al*., 2013). It was recently demonstrated that TIR NADase activity of TNLs upon effector recognition leads to the production of two sets of NAD^+-derived ribosylated nucleotides that preferentially bind to C-terminal grooves of EDS1–PAD4 and EDS1–SAG101 dimers to promote their association with ADR1 and NRG1 helper NLRs ADR1 and NGR1, respectively (Huang *et al*., 2022; Jia *et al*., 2022). In this study, we found that although the $PAD4^{MLF}$ variant interacts very weakly with EDS1 in non-activated tissues, it is fully functional in TNL-triggered *EDS1*-dependent ETI signaling in (Fig. 1). It is conceivable that in TNL-activated tissues, the binding of ribosylated nucleotide small molecules to the EP domain cavity of EDS1–$PAD4^{MLF}$ strengthens this interaction to confer ETI.

Using $PAD4^{MLF}$ as a bait, we identified the papain-like cysteine protease RD19 as an interactor with PAD4 but not SAG101 or EDS1 in transient expression assays both in Arabidopsis protoplasts and *N. benthamiana* (Fig. 2B, C). Consistent with this, RD19 was previously identified as a PAD4 interaction partner in an IP–MS/MS study of bacterial AvrRps4-triggered leaf tissues (Sun *et al*., 2021). Thus, RD19 interacts with PAD4 in non-triggered and immune-activated tissues. Notably, the presence of EDS1 reduced PAD4 interaction with RD19 (Fig. 2D), suggesting that the strong direct association between EDS1 and PAD4 limits the free pool of PAD4 for interaction with RD19. Co-IP experiments testing interactions between RD19 and PAD4–SAG101 chimeric proteins revealed that the N-terminal domain of PAD4 is responsible for its association with RD19 (Fig. 2E). While the MLF mutation of N-terminal PAD4 substantially reduced PAD4 association with EDS1 (Fig. 1E), it did not strongly impact PAD4–RD19 interaction (Fig. 2A). It is therefore likely that PAD4 uses different N-terminal surfaces to interact with RD19 or EDS1.

RD19 was shown to promote TNL RRS1/RPS4-mediated ETI to *R. solanacearum* expressing effector PopP2 (Bernoux *et al*., 2008). Our pathogen infection assays demonstrated that RD19 and RD19c positively regulate RRS1/RPS4-mediated resistance to *P. syringae* expressing a different RRS1/RPS4-recognized effector, AvrRps4 (Fig. 3A). However, the *rd19 rd19c* double mutant had no detectable role in TNL *RPP4*-mediated immunity to *Hpa* isolate Emwa1 (Supplementary Fig. S3), which is strongly *PAD4*-dependent (van der Biezen *et al*., 2002). Moreover, the *rd19* and *rd19c* mutants showed enhanced susceptibility to virulent powdery mildew fungal infection (Fig. 3B, C), but not to virulent *Pst* DC3000 bacteria (Supplementary Fig. S3C). Therefore, it seems that RD19 PLCPs are necessary for only a subset of TNL-ETI and basal resistance responses. This might be explained by differential effectiveness of RD19 PLCP activities against pathogens with varying effector panels and infection strategies. Alternatively, induced expression of *RD19* and *RD19c* (Supplementary Fig. S2B, C) might be below a threshold to contribute measurably to RPP4-mediated ETI to *Hpa* Emwa1 or basal resistance against *Pst* DC3000.

The apoplastic cysteine protease Rcr3 from tomato functions as a decoy to trap the fungal effector Avr2. As the Rcr3–Avr2 protein complex is recognized by the cell-surface receptor-like protein Cf-2 to trigger resistance to fungal pathogen *Cladosporium fulvum*, the proteolytic activity of Rcr3 is not required for the Cf-2-mediated immune response. Unlike Rcr3, our genetic studies of catalytic triad mutations $RD19^{C159A}$ and $RD19^{N329A}$ indicate that the protease activity of RD19 is required for its function in promoting immunity (Fig. 5). Therefore, it is possible that one or more substrates of RD19 are negative regulators of plant immunity, or a substrate of RD19 is guarded by a TNL receptor for ETI activation.

As a papain-like cysteine protease, RD19 contains an N-terminal signal peptide and an auto-inhibitory pro-domain. The predicted mature form of RD19 contains 235 amino acids ($RD19^{134–368}$) with a molecular mass of 25 kDa. However, immunoblots detected only two bands of RD19–FLAG approximately at 41 kDa and 44 kDa (Fig. 4A; Supplementary S4A), and no detectable band below 40 kDa (Supplementary Fig. S4). We propose that the lower band at 41 kDa is proRD19, an intermediate form of RD19 without its signal peptide (Fig. 7A). The presence of proRD19 is dependent on its protease activity (Fig. 5B), indicating that RD19 likely undergoes a self-processed maturation. It has been reported that epitope tags on papain-like cysteine proteases are frequently degraded in the proteolytic environment created when proteases are overexpressed (Richau *et al*., 2012). Therefore, it is also possible that the mature form of RD19 (~25 kDa) in the OE-RD19 lines lost its C-terminal FLAG tag and thus was undetectable on the immunoblots (Supplementary Fig. S4A).

How maturation of papain-like cysteine proteases is achieved is largely unknown. Here, our results show that PAD4 interacts with RD19 via the PAD4 N-terminal lipase-like domain (Fig.2). Importantly, accumulation of processed RD19 (proRD19) was greatly reduced in *pad4-1* mutant (Fig. 6A), suggesting that PAD4 influences maturation of RD19, either by facilitating RD19 maturation directly or by re-localizing RD19 to a compartment where proRD19 is stabilized. Moreover, both *PAD4* and *EDS1* are genetically required for *RD19* overexpression-mediated autoimmunity and enhanced basal resistance (Fig. 6). Considering that protease activity is required for RD19-promoted immunity (Fig. 5), we speculate that RD19–PAD4 (as phase 1) and then PAD4–EDS1 (as phase 2) create a defense-potentiation loop. Such a feedback loop created by PLCPs and SA has been reported in maize (Ziemann *et al.*, 2018). Treatment with SA in *Zea mays* led to the activation of two apoplastic PLCPs, CP1 and CP2, which cleaved and released an immunogenic peptide, Zip1 (*Z. mays* IMMUNE SIGNALLING PEPTIDE 1). Zip1 in turn strongly elicited SA accumulation in leaves (Ziemann *et al.*, 2018). In our study, PAD4 promoted the maturation of RD19 in *RD19* overexpression lines (Fig. 6A). The activated RD19 might lead to the degradation of negative components and/or up-regulation TIRs or TNLs, resulting in increased production of small molecules that would promote EDS1–PAD4 defense (Fig. 7F).

The subcellular localization of immune regulators is crucial for tight control of the immune system (Cui *et al.*, 2015). Transient expression in *N. benthamiana* leaves showed that overexpressed RD19–YFP was mainly localized in mobile vesicles (Fig. 7C) (Bernoux *et al.*, 2008), whereas proRD19–YFP had a clear fluorescence signal in the nucleus (Fig. 7C). Notably, proRD19 interacted with PAD4 more strongly than its full-length form (Fig. 7B). Moreover, PAD4 influenced the nuclear accumulation of proRD19 (Fig. 7D, E). Taken together, this study suggests that PAD4 alone has a capacity to interact with RD19 and promote its maturation and nuclear accumulation. Because we were not able to track the fully mature RD19 form, we do not exclude the possibility that active RD19 protease has targets in multiple compartments, including the apoplast (van der Hoorn, 2008). As the protease activity of RD19 is required for its function in promoting defense responses (Fig. 5), the identification of RD19 substrates would help to clarify the molecular mechanism by which RD19 regulates plant immunity.

Supplementary data

The following supplementary data are available at *JXB* online.

Fig. S1. RD19 interacts with the PAD4 N-terminal domain.

Fig. S2. Analysis of *RD19* family genes.

Fig. S3. *RD19* and *RD19C* are dispensable for TNL RPP4-mediated ETI and basal defense to bacterial pathogen *Pst* DC3000.

Fig. S4. Protein accumulation and transcription of *RD19* in the transgenic Arabidopsis lines.

Fig. S5. Protein accumulation of two forms of RD19–FLAG in the transgenic lines in different genetic background.

Fig. S6. Nuclear localization signal (NLS) predictions in RD19.

Table S1. Primers used in this study.

Table S2. The PAD4^{MLF}-associated proteins identified by liquid chromatography followed by tandem mass spectrometry (LC–MS/MS).

Acknowledgements

We thank the protein mass spectrometry service group (Group leader Dr Hirofumi Nakagami) at the Max Planck Institute for Plant Breeding Research for LC–MS-based protein identification, and Prof. Dingzhong Tang and Dr Hua Shi for useful discussions and suggestions.

Author contributions

YZ, JEP, and HC designed the experiments. YZ, ZZ, GH, and JL performed most experiments. JS and JB generated transgenic lines expressing *PAD4*^{MLF} and performed pathogen assays on them. LX, HC, GH, and JEP wrote the manuscript.

Conflict of interest

The authors declare no conflict of interest.

Funding

The work was supported by the National Natural Science Foundation of China (NSFC, 31970281; HC), the Max-Planck Society, an International Max-Planck Research School (IMPRS) fellowship to GH and Deutsche Forschungsgemeinschaft (German Research Foundation, SFB-1403-414786233; JEP).

Data availability

All data generated or analysed during the present study can be found within the manuscript and its supplementary data.

References

Ahn HK, Lin X, Olave-Achury AC, Derevnina L, Contreras MP, Kourelis J, Wu CH, Kamoun S, Jones JDG. 2023. Effector-dependent activation and oligomerization of plant NRC class helper NLRs by sensor NLR immune receptors Rpi-amr3 and Rpi-amr1. The EMBO Journal **42**, e111484.

Albert I, Hua C, Nurnberger T, Pruitt RN, Zhang L. 2020. Surface sensor systems in plant immunity. Plant Physiology **182**, 1582–1596.

Bartsch M, Gobbato E, Bednarek P, Debey S, Schultze JL, Bautor J, Parker JE. 2006. Salicylic acid-independent ENHANCED DISEASE SUSCEPTIBILITY1 signaling in *Arabidopsis* immunity and cell death is regulated by the monooxygenase FMO1 and the Nudix hydrolase NUDT7. The Plant Cell **18**, 1038–1051.

Bernoux M, Timmers T, Jauneau A, Briere C, de Wit PJ, Marco Y, Deslandes L. 2008. RD19, an Arabidopsis cysteine protease required for RRS1-R-mediated resistance, is relocalized to the nucleus by the *Ralstonia solanacearum* PopP2 effector. The Plant Cell **20**, 2252–2264.

Bi G, Su M, Li N, *et al*. 2021. The ZAR1 resistosome is a calcium-permeable channel triggering plant immune signaling. Cell **184**, 3528–3541.e12.

Chen H, Zou Y, Shang Y, Lin H, Wang Y, Cai R, Tang X, Zhou JM. 2008. Firefly luciferase complementation imaging assay for protein-protein interactions in plants. Plant Physiology **146**, 368–376.

Clough SJ, Bent AF. 1998. Floral dip: a simplified method for Agrobacterium-mediated transformation of *Arabidopsis thaliana*. The Plant Journal **16**, 735–743.

Contreras MP, Pai H, Tumtas Y, *et al*. 2023. Sensor NLR immune proteins activate oligomerization of their NRC helpers in response to plant pathogens. The EMBO Journal **42**, e111519.

Cui H, Qiu J, Zhou Y, Bhandari DD, Zhao C, Bautor J, Parker JE. 2018. Antagonism of transcription factor MYC2 by EDS1/PAD4 complexes bolsters salicylic acid defense in *Arabidopsis* effector-triggered immunity. Molecular Plant **11**, 1053–1066.

Cui H, Tsuda K, Parker JE. 2015. Effector-triggered immunity: from pathogen perception to robust defense. Annual Review of Plant Biology **66**, 487–511.

Dongus JA, Bhandari DD, Patel M, Archer L, Dijkgraaf L, Deslandes L, Shah J, Parker JE. 2020. The *Arabidopsis* PAD4 lipase-like domain is sufficient for resistance to green peach aphid. Molecular Plant-Microbe Interactions **33**, 328–335.

Dongus JA, Bhandari DD, Penner E, *et al*. 2022. Cavity surface residues of PAD4 and SAG101 contribute to EDS1 dimer signaling specificity in plant immunity. The Plant Journal **110**, 1415–1432.

Dongus JA, Parker JE. 2021. EDS1 signalling: at the nexus of intracellular and surface receptor immunity. Current Opinion in Plant Biology **62**, 102039.

Engler C, Youles M, Gruetzner R, Ehnert TM, Werner S, Jones JD, Patron NJ, Marillonnet S. 2014. A golden gate modular cloning toolbox for plants. ACS Synthetic Biology **3**, 839–843.

Feys BJ, Wiermer M, Bhat RA, Moisan LJ, Medina-Escobar N, Neu C, Cabral A, Parker JE. 2005. *Arabidopsis* SENESCENCE-ASSOCIATED $GENE_{101}$ stabilizes and signals within an ENHANCED DISEASE $SUSCEPTIBILITY_1$ complex in plant innate immunity. The Plant Cell **17**, 2601–2613.

Forderer A, Li E, Lawson AW, *et al*. 2022. A wheat resistosome defines common principles of immune receptor channels. Nature **610**, 532–539.

Frye CA, Innes RW. 1998. An Arabidopsis mutant with enhanced resistance to powdery mildew. The Plant Cell **10**, 947–956.

Gantner J, Ordon J, Kretschmer C, Guerois R, Stuttmann J. 2019. An EDS1-SAG101 complex is essential for TNL-mediated immunity in *Nicotiana benthamiana*. The Plant Cell **31**, 2456–2474.

Godson A, van der Hoorn RAL. 2021. The front line of defence: a meta-analysis of apoplastic proteases in plant immunity. Journal of Experimental Botany **72**, 3381–3394.

Heidrich K, Tsuda K, Blanvillain-Baufume S, Wirthmueller L, Bautor J, Parker JE. 2013. *Arabidopsis* TNL-WRKY domain receptor RRS1 contributes to temperature-conditioned RPS4 auto-immunity. Frontiers in Plant Science **4**, 403.

Hu Z, Chai J. 2023. Assembly and architecture of NLR resistosomes and inflammasomes. Annual Review of Biophysics **52**, 207–228.

Huang S, Jia A, Song W, *et al*. 2022. Identification and receptor mechanism of TIR-catalyzed small molecules in plant immunity. Science **377**, eabq3297.

Ilyas M, Horger AC, Bozkurt TO, *et al*. 2015. Functional divergence of two secreted immune proteases of tomato. Current Biology **25**, 2300–2306.

Jia A, Huang S, Ma S, Chang X, Han Z, Chai J. 2023. TIR-catalyzed nucleotide signaling molecules in plant defense. Current Opinion in Plant Biology **73**, 102334.

Jia A, Huang S, Song W, *et al*. 2022. TIR-catalyzed ADP-ribosylation reactions produce signaling molecules for plant immunity. Science **377**, eabq8180.

Jiang Y, Ding P. 2023. Calcium signaling in plant immunity: a spatiotemporally controlled symphony. Trends in Plant Science **28**, 74–89.

Jirage D, Tootle TL, Reuber TL, Frost LN, Feys BJ, Parker JE, Ausubel FM, Glazebrook J. 1999. *Arabidopsis thaliana* PAD4 encodes a lipase-like gene that is important for salicylic acid signaling. Proceedings of the National Academy of Sciences, USA **96**, 13583–13588.

Jones JD, Vance RE, Dangl JL. 2016. Intracellular innate immune surveillance devices in plants and animals. Science **354**, aaf6395.

Kim NH, Jacob P, Dangl JL. 2022. Con-Ca^{2+}-tenating plant immune responses via calcium-permeable cation channels. New Phytologist **234**, 813–818.

Koch E, Slusarenko A. 1990. *Arabidopsis* is susceptible to infection by a downy mildew fungus. The Plant Cell **2**, 437–445.

Koster P, DeFalco TA, Zipfel C. 2022. $CaCa^{2+}$ signals in plant immunity. EMBO Journal **41**, e110741.

Lapin D, Bhandari DD, Parker JE. 2020. Origins and immunity networking functions of EDS1 family proteins. Annual Review of Phytopathology **58**, 253–276.

Lapin D, Johanndrees O, Wu Z, Li X, Parker JE. 2022. Molecular innovations in plant TIR-based immunity signaling. The Plant Cell **34**, 1479–1496.

Lapin D, Kovacova V, Sun X, *et al*. 2019. A coevolved EDS1-SAG101-NRG1 module mediates cell death signaling by TIR-domain immune receptors. The Plant Cell **31**, 2430–2455.

Le Roux C, Huet G, Jauneau A, *et al*. 2015. A receptor pair with an integrated decoy converts pathogen disabling of transcription factors to immunity. Cell **161**, 1074–1088.

Li X, Lin H, Zhang W, Zou Y, Zhang J, Tang X, Zhou JM. 2005. Flagellin induces innate immunity in nonhost interactions that is suppressed by *Pseudomonas syringae* effectors. Proceedings of the National Academy of Sciences, USA **102**, 12990–12995.

Liu H, Hu M, Wang Q, Cheng L, Zhang Z. 2018. Role of papain-like cysteine proteases in plant development. Frontiers in Plant Science **9**, 1717.

Locci F, Wang J, Parker JE. 2023. TIR-domain enzymatic activities at the heart of plant immunity. Current Opinion in Plant Biology **74**, 102373.

Louis J, Gobbato E, Mondal HA, Feys BJ, Parker JE, Shah J. 2012. Discrimination of Arabidopsis PAD4 activities in defense against green peach aphid and pathogens. Plant Physiology **158**, 1860–1872.

Ma S, Lapin D, Liu L, *et al*. 2020. Direct pathogen-induced assembly of an NLR immune receptor complex to form a holoenzyme. Science **370**, eabe3069.

Martin R, Qi T, Zhang H, Liu F, King M, Toth C, Nogales E, Staskawicz BJ. 2020. Structure of the activated ROQ1 resistosome directly recognizing the pathogen effector XopQ. Science **370**, eabd9993.

Ngou BPM, Ahn HK, Ding P, Jones JDG. 2021. Mutual potentiation of plant immunity by cell-surface and intracellular receptors. Nature **592**, 110–115.

Parker JE, Hessler G, Cui H. 2022. A new biochemistry connecting pathogen detection to induced defense in plants. New Phytologist **234**, 819–826.

Paulus JK, Kourelis J, Ramasubramanian S, *et al*. 2020. Extracellular proteolytic cascade in tomato activates immune protease Rcr3. Proceedings of the National Academy of Sciences, USA **117**, 17409–17417.

Pegadaraju V, Louis J, Singh V, Reese JC, Bautor J, Feys BJ, Cook G, Parker JE, Shah J. 2007. Phloem-based resistance to green peach aphid is controlled by Arabidopsis PHYTOALEXIN DEFICIENT4 without its signaling partner ENHANCED DISEASE SUSCEPTIBILITY1. The Plant Journal **52**, 332–341.

Pogorelko GV, Juvale PS, Rutter WB, *et al*. 2019. Re-targeting of a plant defense protease by a cyst nematode effector. The Plant Journal **98**, 1000–1014.

Richau KH, Kaschani F, Verdoes M, Pansuriya TC, Niessen S, Stuber K, Colby T, Overkleeft HS, Bogyo M, Van der Hoorn RA. 2012. Subclassification and biochemical analysis of plant papain-like cysteine proteases displays subfamily-specific characteristics. Plant Physiology **158**, 1583–1599.

Rietz S, Stamm A, Malonek S, Wagner S, Becker D, Medina-Escobar N, Vlot AC, Feys BJ, Niefind K, Parker JE. 2011. Different roles of Enhanced Disease Susceptibility1 (EDS1) bound to and dissociated from Phytoalexin Deficient4 (PAD4) in Arabidopsis immunity. New Phytologist **191**, 107–119.

Rooney HC, Van't Klooster JW, van der Hoorn RA, Joosten MH, Jones JD, de Wit PJ. 2005. *Cladosporium* Avr2 inhibits tomato Rcr3 protease required for Cf-2-dependent disease resistance. Science **308**, 1783–1786.

Sarris PF, Duxbury Z, Huh SU, *et al*. 2015. A plant immune receptor detects pathogen effectors that target WRKY transcription factors. Cell **161**, 1089–1100.

Sun X, Lapin D, Feehan JM, *et al*. 2021. Pathogen effector recognition-dependent association of NRG1 with EDS1 and SAG101 in TNL receptor immunity. Nature Communications **12**, 3335.

Tian H, Wu Z, Chen S, *et al*. 2021. Activation of TIR signalling boosts pattern-triggered immunity. Nature **598**, 500–503.

van der Biezen EA, Freddie CT, Kahn K, Parker JE, Jones JD. 2002. Arabidopsis RPP4 is a member of the RPP5 multigene family of TIR-NB-LRR genes and confers downy mildew resistance through multiple signalling components. The Plant Journal **29**, 439–451.

van der Hoorn RA. 2008. Plant proteases: from phenotypes to molecular mechanisms. Annual Review of Plant Biology **59**, 191–223.

Wagner S, Stuttmann J, Rietz S, Guerois R, Brunstein E, Bautor J, Niefind K, Parker JE. 2013. Structural basis for signaling by exclusive EDS1 heteromeric complexes with SAG101 or PAD4 in plant innate immunity. Cell Host and Microbe **14**, 619–630.

Wang J, Hu M, Wang J, Qi J, Han Z, Wang G, Qi Y, Wang HW, Zhou JM, Chai J. 2019. Reconstitution and structure of a plant NLR resistosome conferring immunity. Science **364**, eaav5870.

Wu Z, Tian L, Liu X, Zhang Y, Li X. 2021. TIR signal promotes interactions between lipase-like proteins and ADR1-L1 receptor and ADR1-L1 oligomerization. Plant Physiology **187**, 681–686.

Yuan M, Jiang Z, Bi G, Nomura K, Liu M, Wang Y, Cai B, Zhou JM, He SY, Xin XF. 2021. Pattern-recognition receptors are required for NLR-mediated plant immunity. Nature **592**, 105–109.

Ziemann S, van der Linde K, Lahrmann U, *et al*. 2018. An apoplastic peptide activates salicylic acid signalling in maize. Nature Plants **4**, 172–180.